Available online at www.sciencedirect.com
ScienceDirect
Journal of the European Ceramic Society 31 (2011) 541–548
www.elsevier.com/locate/jeurceramsoc

The effect of room temperature and high temperature exposure on the elastic modulus, hardness and fracture toughness of glass ceramic sealants for solid oxide fuel cells

Yilin Zhao, Jürgen Malzbender*, Sonja M. Gross

Forschungzentrum Jülich GmbH, 52146 Jülich, Germany

Received 10 August 2010; received in revised form 11 October 2010; accepted 27 October 2010
Available online 27 November 2010

Abstract

The reliable operation of solid oxide fuel cell stacks (SOFCs) depends strongly on the structural integrity of the sealing material. Indentation testing is used to determine the mechanical properties of glass-ceramic sealants typically used for solid oxide fuel cell stacks, in particular for the evaluation of elastic modulus, hardness and fracture toughness. Different sealing materials partly with reinforcement by metallic or ceramic filler (particles or short fibers) are tested. The materials are tested after the joining procedure and after additional annealing at operation temperatures to test the effect of further crystallization that might take place. Furthermore, the effect of environmentally enhanced slow crack growth at low temperatures in water saturated atmosphere is investigated. Finally, self-healing effects of the glass ceramic materials with and without pre-annealing at typical operation temperatures are considered.

Keywords: Mechanical properties; Glass ceramic; Indentation; Fracture; Fuel cells

1. Introduction

One of the most important challenges in the fabrication and commercialization of planar SOFCs is the development of reliable and robust sealant materials that survive long term operation and thermal cycling. Joining and sealing techniques can be based on joining with glass, glass ceramics or glass composite sealants.[1–3] Glasses and glass ceramics appear to have better resistance to both oxidizing and reducing environments than metallic sealants and can fulfill most of the requirements that need to be exhibited by an ideal sealing material. In particular the sealant should hermetically separate anode and cathode gas supply and be chemically stable to any component materials, with which it is in contact in oxidizing and reducing atmospheres, possessing sufficient bonding strength.[1] Glass ceramic materials are generally cheap; can be applied to the sealing surfaces as a powder dispersed in a paste or as tape cast sheets; typically exhibit good wetting behavior on both sealing surfaces; are electrically insulating; can be engineered to exhibit a coefficient of thermal expansion (CTE) matching those of the adjacent SOFC components in the final joint, thereby minimizing thermally induced stresses.[2,4]

The most important criteria for the selection of a suitable sealant are the glass transition temperature and the coefficient of thermal expansion.[4] Glasses and partially crystallized glass ceramics possess such a transition temperature, below which the material changes from ductile to brittle behavior. The glass transition temperature is important because even if crystallization takes place in a later stage of the sealing process, the initial glass must flow sufficiently to provide an adequate joint.[5] During the joining, the glass might partially or fully crystallize to form a rigid, bonded seal. Crystallization is advantageous since the resulting material is typically mechanically stronger than the initial glass. However the final joint is brittle and susceptible to fracture when exposed to tensile stresses that might occur due to thermal cycling as a result of thermal expansion mismatches between the sealant and adjacent substrates or simply operational temperature gradients.[6]

Although stresses might be released by viscous creeping, another challenge is to stabilize the glass-ceramic material's CTE as a function of time at elevated temperatures. It is

* Corresponding author. Tel.: +49 2641 616964; fax: +49 2461 613699.
E-mail address: j.malzbender@fz-juelich.de (J. Malzbender).

0955-2219/$ – see front matter © 2010 Elsevier Ltd. All rights reserved.
doi:10.1016/j.jeurceramsoc.2010.10.032

possible to stabilize the long term CTE by changing the starting composition or by introducing filler additions.

Another task is to control the reactivity of glass ceramic sealants with the metallic components. For example, barium–calcium–alumino-silicate sealants generally adhere well to YSZ with little chemical interaction, but tend to form interfacial reaction products with the oxide scales of the metallic interconnect at the typical stack operating temperatures, and these phases might thicken and become porous yielding interfaces that can be weak and susceptible to thermo-mechanically induced cracking.[7] Particle or fiber reinforcements are considered one effective way of optimization the fracture toughness by crack stopping and deflection. The filler could be either a brittle material with high elastic modulus and toughness or a ductile material, since the filler materials can raise the energy for the crack growth by their plastic deformation whereas brittle materials absorb all the energy during pulling out of, for example the fiber from matrix. Additionally the crack path can be extended due to the stress field surrounding the filler material.

The brittleness of the glass and glass ceramic based seals has been reported to be one of the main problems for seals; hence it is important to assess the mechanical properties of the material. Indentation has been used widely to measure the hardness H of materials. It is also possible to obtain the elastic modulus E from the load–displacement data and the fracture toughness K_{IC} from cracks forming when a certain threshold load is exceeded.[8]

In fact, it is known that for glasses cracks grow slowly even at room temperature. This phenomenon is called slow crack growth or sometimes also fatigue. It may have large implications for the lifetime of a component, and it is therefore very important to take this effect into consideration.[9] The main reason of slow crack growth (SCG) is stress-assisted chemical reactions at the crack tip. Pre-existing surface flaws grow slowly under stress to a critical length at which unstable rapid crack propagation occurs, leading to catastrophic failure. The time to failure is a function of the applied stress for a given material and ambient environment; the smaller the applied stress, the longer the time to fracture. The same material can show totally different behavior in the dry and in the wet atmosphere. The slow crack growth takes place in humid atmosphere, since glass reacts with water and under the combined action of a residual stress near a crack tip and with this chemical reaction, the crack may grow in time under subcritical conditions. When the applied stress diminishes to a threshold level, known as a fatigue limit, failure of the solid can be avoided. The existence of such a limit has been verified for just a few materials. In the case of glass it has been estimated as 0.17 times the value of K_{IC}.

Different sealant materials partly reinforced by metallic or ceramic filler (particles or short fibers) are characterized with respect to their hardness, elastic modulus and fracture toughness as obtained using indentation testing. The sealant materials are tested after the usually applied joining procedure and additional annealing at operation temperature to test the effect of further crystallization that might take place. Furthermore, the effect of environmentally enhanced slow crack growth at low temperatures in water saturated atmosphere is tested. Finally, self-healing effects of the glass-ceramic materials with and without pre-annealing at typical operation temperatures are considered. Within the composition ranges studied during the present investigation an optimum composition is suggested that could act as a useful sealing material for SOFC.[10]

Table 1
The chemical composition of glass H.

in wt.%	BaO	SiO_2	CaO	Additions
Glass H	48.2	29.8	6.1	Al_2O_3, B_2O_3, V_2O_5, ZnO

2. Experiments

2.1. Composite sealant preparation based on glass H

This composite sealant is based on a glass matrix of the BaO–CaO–SiO_2 ternary system with addition of small amounts of Al_2O_3, B_2O_3, V_2O_5, ZnO (Table 1). The raw materials were obtained from Merck KGaA Darmstadt and had a grade of purity higher than 99%. Each batch is prepared by mixing an appropriate mole fraction of oxide ingredients, and melting at 1480 °C in a platinum crucible in an induction furnace.[3] For a better homogenization of the glass, the melting procedure is carried out twice. For making powder, the frits were wet-milled in acetone in an agate ball mill to a median particle size of 10–13 μm, dried and then sieved through a mesh size of 0.32 μm to collect powders. The chemical composition of sample is analyzed by inductively coupled plasma optical emission spectroscopy (ICP-OES, Table 1).

To obtain a bulk glass sample, the melt is poured into a graphite mould and transferred to a preheated (750 °C) chamber furnace as soon as it is dimensionally stable, followed by slow cooling to room temperature.

To obtain sintered rods, the powders were either pressed and sintered and annealed without filler (GC-H) or mixed separately with YSZ particles (GC-HYSZ), YSZ fibers (GC-HZYBF) and silver particles (GC-HAg), respectively, pressed and sintered at 850 °C for 10 h and then either cooled down to RT (initial state) or to 800 °C and left for 500 h before cool down to RT. Heating and cooling rate was always 5 K/min.

2.2. Crystallizing sealant preparation of glass B

The glass ceramic sealant B is based on a glass of the system BaO–CaO–SiO_2 with addition of Al_2O_3 and received the same processing as GC-H series. After the melting and wet milling, some of the glass B powder was taken for CTE measurement. Chemical composition of sample has been analyzed by inductively coupled plasma optical emission spectroscopy (ICP-OES, Table 2). Glass B powder was pressed and sintered at 950 °C

Table 2
Chemical composition of glass B.

in wt.%	BaO	SiO_2	CaO	Additions
Glass B	36.7	46.8	15.8	Al_2O_3

for 10 h then either cooled down to RT or annealed for 100 h, 500 h, 1000 h at 800 °C, the typical stack operation temperature. Heating and cooling rate was always 5 K/min.

2.3. Elastic modulus, hardness and fracture toughness measurements

The hardness H and elastic modulus of a material are determined on the basis of the following relationships:[8]

$$H = \frac{F_{\max}}{A_C} \tag{1}$$

$$E* = \frac{\sqrt{\pi} \cdot S_{\max}}{\sqrt{4 \cdot A_C}} \tag{2}$$

$$\frac{1}{E*} = \frac{1 - \nu_i^2}{E_i} + \frac{1 - \nu^2}{E} \tag{3}$$

where F_{max} is the Force that applied to the material and A_c is the contact area. The reduced Young's Modulus E^* is expressed in terms of the unloading slope of the indentation load displacement curve S_{max}, the modulus and Poisson's ratio of the indenter E_i and ν_i, and the modulus and Poisson's ratio of the to be investigated material E and ν.

The indentation tests were carried out at RT. Before the measurements the specimens were prepared by the standard metallographic technique. The samples were cut into small pieces (Linear Precision Saw), then, mounted with Demote 33 epoxy resin, grounded with SiC papers from grade 240 to 4000 and then polished up from 0.3 μm to 0.1 μm, with a diamond paste and final polishing with silica suspension, improving their reflectivity.

A Fischer indenter (H100C) and CSM microindenter (CSM instrument, Switzerland) were used with Vickers diamond tips, the resolution of the measurement was 0.1 μm. The machines have been calibrated with fused silica ($\nu = 0.17$ and $E = 72$ GPa). The hardness and elastic modulus was tested with 25 indents each at loads of 10 mN, 100 mN, 300 mN, 500 mN and 1000 mN, respectively. The fracture toughness K_{IC} has been measured from the traces of the radial cracks in the surface that occur due to the indentation using:[8]

$$K_{IC} = \chi \frac{P}{c^{1.5}} \tag{4}$$

where c is the length of the radial crack, and χ is a indenter constant that also depends on elastic modulus and hardness of the tested material.

For the crack healing at high temperature all specimens (at non-aged and aged state) were polished and then indented with loads of 5 N and 10 N using a Vickers indenter. All materials of the GC-H series were reheated first to 800 °C annealed for 24 h and then cooled (rate 5 K/min) to RT. Then the crack length was re-measured. In subsequent steps the materials were annealed to 850 °C and 900 °C using the same procedure. The indentation cracks for the GC-B specimens were re-examined after annealing at 900 °C and 950 °C.

2.4. Phase and microstructure identification (XRD, SEM)

Crystalline phases of the glass ceramics before and after 500 h annealing were examined by X-ray diffraction at ambient temperature using a step scan procedure (0.02°/2θ step, count time 5 s) with a crystal monochromator employing Cu-Ka radiation. The microstructure of the polished cross-sections of the non-aged and aged glass ceramics were examined using a Zeiss Ultra 55 scanning electron microscope (SEM). The fracture surfaces after immediately indentation (loads 2 N, 5 N), after slow crack growth and crack healing are examined by optical microscope.

3. Results

3.1. Microstructure investigation

X-ray diffraction patterns have been obtained for all specimens. Being representative for the GC-H series, Fig. 1 shows as an example the XRD patterns for the GC-HYSZ in the initial state and after 500 h annealing. The number of peaks increases after annealing indicating progressive crystallization with the formation of new phases. The high background with a raise of the baseline of θ between 20 and 35 is an indication of a high content of amorphous phase, especially in the initial state. The new crystalline phase $CaSrAl_2SiO_7$ appeared in the aged GC-HYSZ in addition to the $Ba_{0.808}(Al_{1.71}Si_{2.29})O_8$, $Ba_5Si_8O_{21}$ and $ZrO_{1.95}$ crystalline phases which exist in the initial material. The XRD patterns of non-aged and aged GC-H are similar to non-aged and aged GC-HYSZ. However, for the GC-HZYBF no new crystalline phases appear after annealing.

Microstructural SEM images of the non-aged and aged GC-HYSZ are given in Fig. 2. For the non-aged GC-HYSZ, these micrographs show white flakes of binary barium silicates and dark grey bars of barium–alumino-silicates which appear to be crystalline phases while the residual glass is the grey region. The big white structures are YSZ particles and there are some micro-voids which are generated during the preparation process. In spite of the availability of large interface areas between the YSZ particles and the glass matrix, the glass nucleates and crystallizes rather independently of these particles. After 500 h heat treatment for the aged GC-HYSZ, volume and grain boundary diffusion takes place. The newly formed crystalline phases are randomly distributed within the remaining glassy matrix. With exception of the big white particles, the fine and uniform crystalline structure and micro-voids are the main characteristics. There is still a significant amount of residual glassy phase. The volume fractions of the remaining glassy phases measured by the line intercept method after ASTM standard E 112 from the SEM micrographs are given in Table 3.

Table 3
Volume fraction in % of glassy phase (±5%).

Material	GC-H	GC-HYSZ	GC-HZYBF	GC-HAg	GC-B
Initial state	75	83	91	46	6
Aged	41	63	75	21	5

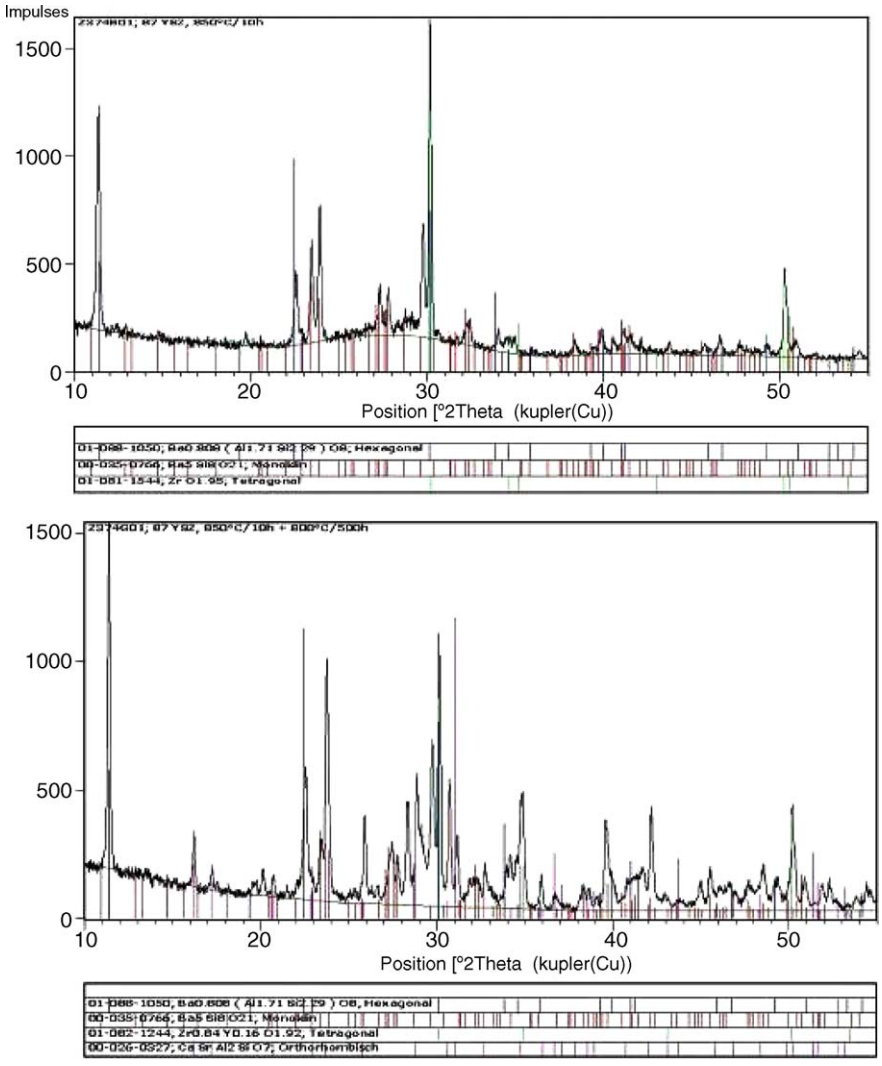

Fig. 1. XRD of GC-HYSZ (a) in the initial state and (b) after annealing at 800 °C for 500 h.

The volume fraction of the glassy phase decreases with the annealing time for all the specimens, except GC-B. The materials already partially crystallize during the initial heat treatment. For GCH, GCH-ZYBF and GCH-YSZ the fraction volume of glassy phase is around 80% in the initial state, whereas GC-HAg has only 46% glassy phase. After an additional annealing for 500 h at 800 °C the volume fraction is still around 75% for GC-HZYBF and 63% for GC-HYSZ which means that the amorphous glass remains the main phase. The values of GC-H and GC-Ag decreases to approximately 41% and 21%, respectively, implying that the glassy phase is here not the main phase anymore. Micro-cracks that can be observed in the aged material might be related to specimen preparation, however can also be a result of the differences in thermal expansion between the crys-

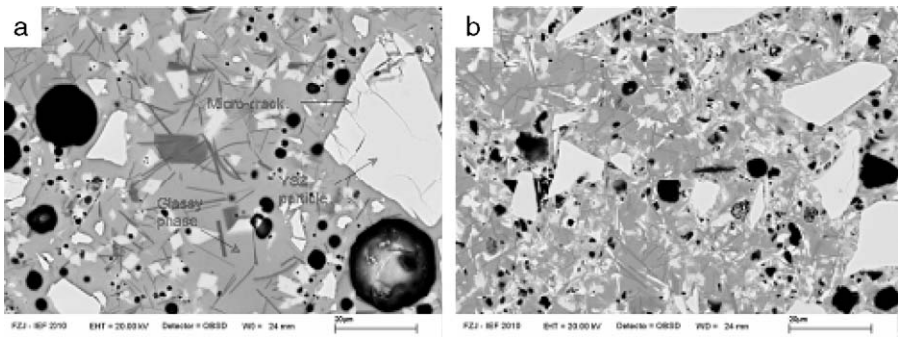

Fig. 2. SEM images of GC-HYSZ (a) initial state and (b) aged at 800 °C for 500 h.

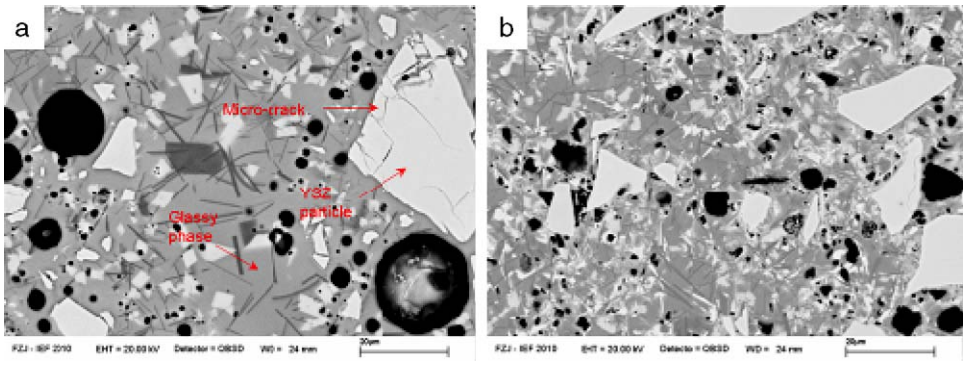

Fig. 3. SEM images of GC-HAg (a) initial state and (b) aged at 800 °C/500 h.

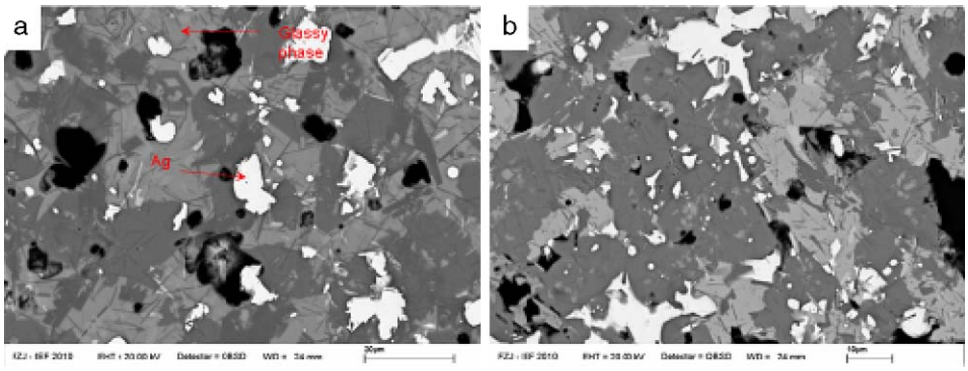

Fig. 4. SEM images of the GC-H series after annealing, (a) GC-H and (b) GC-HZYBF.

talline phases and residual glass. For the non-aged GC-HAg, the strong amorphous nature of the material disappeared after aging. Three new crystalline phases are produced which do not contain the silver element, that means the silver particles are not involved in any reaction with the matrix material. The XRD of the aged GC-HAg is different from other GC-H series, as the crystalline phase $CaSrAl_2SiO_7$ occurred in the initial GC-HAg disappeared after aging. The white cotton-like areas shown in Fig. 3 are silver, which is disposed randomly within the light grey glassy matrix. After 500 h aging, the silver particles are deformed and the dark grey phase increases in volume.

For the GC-B, the XRD spectra showed the same pattern for the non-aged and 500 h aged specimens. No new crystalline phase form after 500 h annealing. The volume fraction of the crystalline phase is around 94%. This implies that the material crystallized fast during the sintering at 950 °C for 10 h. The volume fraction of crystalline phase is basically unchanged after an additional annealing for 500 h at 800 °C verifying that the main crystallization happens during the initial sealing step for GC-B.

The microstructure of the aged GC-H series is illustrated in Fig. 4. More homogenous phases and increasing densification are visible. All the GC-H series in the initial state show sim-

Table 4
E, H and K_{IC} values of GC-H series and GC-B.

Material		Properties					
		E (GPa)	±	H (GPa)	±	K_{IC} (MPa m$^{0.5}$)	
Initial state	H	72	5	5.6	0.7	0.99	0.21
	HYSZ	73	8	5.5	1.2	0.92	0.22
	HZYBF	74	5	6.21	0.7	0.82	0.16
	HAg	75	5	4.2	0.8	1.1	0.03
	4B	77	3	7.2	0.5	0.64	0.04
Aged state	H	80(+11%)	9	5.5(−2%)	1.3	1.12(+13%)	0.15
	HYSZ	79(+10%)	6	5.1(−7%)	0.9	1.5(+63%)	0.12
	HZYBF	86(+16%)	5	6.5(+5%)	0.8	1.3(+59%)	0.14
	HAg	74(−1%)	8	3.4(14%)	1	1.55(+40%)	0.15
	B100 h	73(−5%)	1	7.1(−1%)	0.2	0.61(−5%)	0.13
	B500 h	77(+10%)	3	7.5(+4%)	0.5	0.69(+8%)	0.05
	B100 h	80(+4%)	3	7.7(+7%)	1.5	0.65(+2%)	0.04

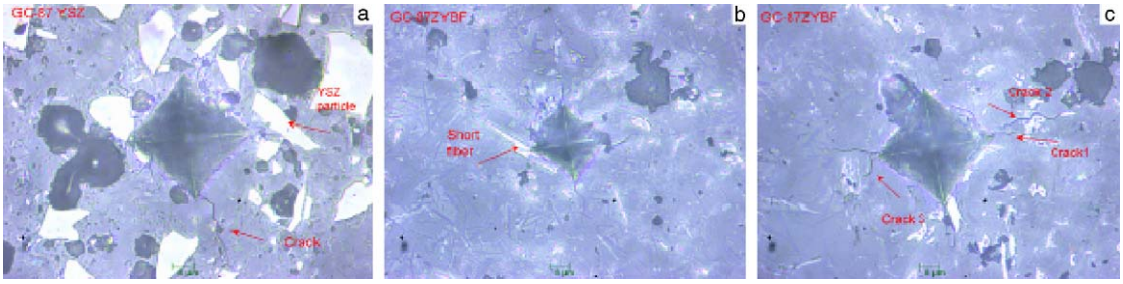

Fig. 5. Examples of micrographs of indentation crack in the fiber and particle reinforced material (a) aged GC-HYSZ (5 N), (b) GC-HZYBF (2 N) and (c) aged GC-HZYBF (5 N).

ilar porosities, significantly larger than for GC-B. After 500 h annealing, GC-HZYBF shows the highest densification and the finest pore structure of the H series.

3.2. Elastic modulus, hardness and fracture toughness

Table 4 summarizes the ambient temperature mechanical properties of the materials in the initial state and after 500 h additional annealing. In the initial state, all the GC-H series and GC-B have elastic modulus values between 72 and 77 GPa, respectively. The values for GC-B are at the higher end of this range (77 ± 3 GPa), which might be associated with the lower amount of glassy phase and small porosity of this material. After 500 h aging, the elastic moduli of GC-H, GC-HYSZ and GC-HZYBF increase between 10% and 16%. This can be associated with progressing crystallization as discussed above. The minor changes for the other specimens are within the limits of uncertainty. There was no load dependence of the elastic modulus within a range of 10–500 mN. After annealing, GC-HZYBF has the highest stiffness, which might be associated with crystallization or decreasing porosity.

GC-HAg in the initial state shows the lowest hardness value of about 4.2 GPa due to the ductility of the Ag particle. The materials GC-HZYBF and GC-B possess the highest values, which can be associated with the fiber reinforcement and the stronger crystallization, respectively. After 500 h annealing, the hardness of GC-HAg decreases significantly by 14% and considering the SEM images it appears that the Ag is deformed now along the grain boundaries offering an easier means of deformation.

For the all indented specimens, crack became visible at ~300 mN. Typical crack morphologies are illustrated in Fig. 5. The GC-H series with and without filler have almost the same fracture toughness in the initial state with values lower than 1.0 MPa $m^{0.5}$ (Table 4), however, still being higher than GC-B with ~0.6 MPa $m^{0.5}$. Whereas the fracture toughness for GC-H series with filler increased clearly by values between 40% and 60% the values for GC-H and GC-B were basically unchanged. Hence, in agreement with the SEM observation on the crystallization, particle and fiber reinforcement have a significant effect on the fracture toughness.

The indentation crack formed in GC-HYSZ (Fig. 5) stops at the YSZ particles. For GC-HZYBF the cracks marked as 1 and 3 in Fig. 5(c) are stopped by the short fibers, and crack 2 bypass the fiber obstacles in front of it. Hence it is considered that bridging and crack deflections act as toughening or strengthening mechanisms.

3.3. Slow crack growth at low temperature

Water or humidity can act as corrosive agent for glasses by destroying the oxygen–silicon network. Under normal conditions, the corrosion of glass proceeds very slowly, however, can be promoted significantly by mechanical stress. The slow crack growth rate (SCGR) at room temperature after two weeks in ambient air for the CG-H series and CG-B were very low (0.2–0.3%). To increase the SCGR further experiment were carried under a water saturated atmosphere at 40 °C for 40 h, before the crack length was re-measured for indentation cracks (loads 2 N, 5 N and 10 N).

The GC-H materials with filler appear to have larger SCGR rates (Table 5). Furthermore, for the H series the aging does not change the SCGR and the glassy phase might still dominate the behavior. The GC-B shows slightly higher values than the GC-H without filler. For the GC-B additional experiments were carried out with specimens that received shorter and longer pre-annealing, revealing the SCGR decreased for specimens that received longer pre-annealing ($18 \pm 10\%$ for 100 h, $4 \pm 1\%$ for 1000 h). The results might imply higher slow crack growth rates for the GC-H series in comparison to GC-B. However, further experiments are needed for confirmation.

Fig. 6 shows the non-aged GC-HYSZ before and after the slow crack growth test. The arrows illustrate that the crack propagates during the 5 days. The radial crack on the right side grows around the YSZ particle and connects with another lateral crack indicating that the YSZ particles is tougher than the glass matrix. Fig. 7 shows the result of the aged GC-H and GC-HZYBF, respectively. The radial cracks for the aged GC-H indicated by an arrow propagated surpassing a pore. For GC-HZYBF, the cracks grow distinctively. Fig. 8 displays GC-B initially aged

Table 5
Average SCGR after 5 days exposure to saturated atmosphere at 40 °C.

SCGR (%) of glass ceramic	Initial state	Aged (500 h)
H	6 ± 4	9 ± 1
HAg (Ag reinforcement)	21 ± 11	20 ± 6
HYSZ (YSZ particle reinforcement)	29 ± 15	23 ± 4
HZYBF (YSZ short fibers)	24 ± 12	24 ± 4
B	12 ± 8	13 ± 3

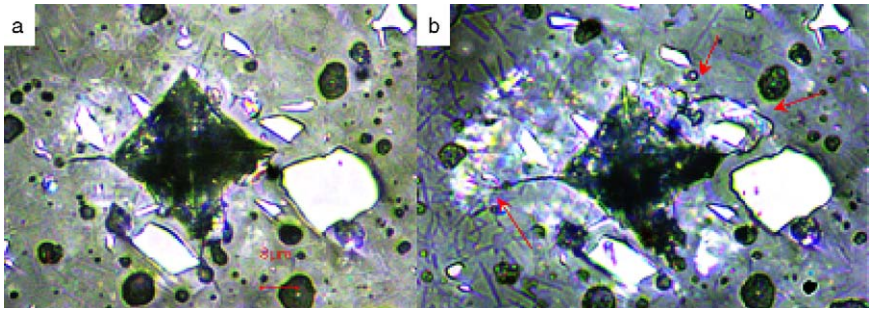

Fig. 6. Indentation for GC-HYSZ (not aged, 2 N) (a) initial impression (b) after SCG.

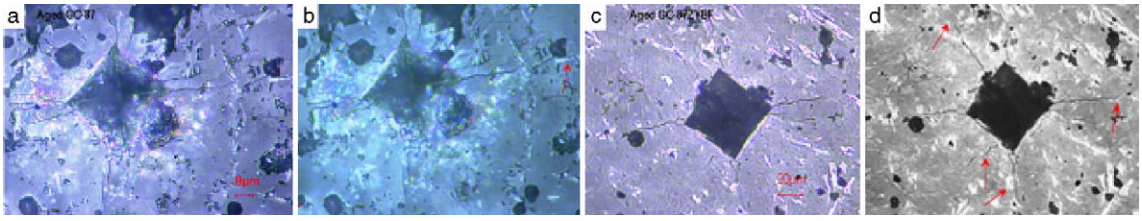

Fig. 7. Indentation for GC-H (aged, 5 N) (a) initial impression, (b) after SCG and GC-HZYBF (aged, 10 N), (c) initial impression and (d) after SCG.

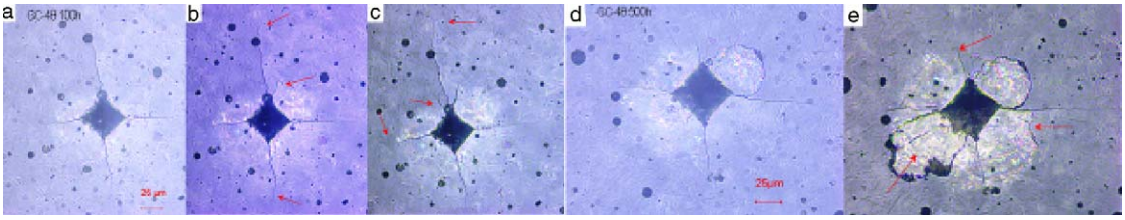

Fig. 8. Indentation of 100 h aged GC-B (a) initial stage, (b) after 3 days SCG and (c) after 5 days SCG, (d) initial indentation of 500 h aged GC-B and (e) after 3 days SCG.

100 h and 500 h, respectively, after the slow crack growth test. For GC-B aged 100 h, the radial crack propagated by branching from the edge of the impression. The specimen aged 500 h shows in addition to radial crack growths also the growth of a lateral (delamination) crack.

3.4. Self-healing at operation temperature

All materials of the GC-H series and GC-B behave as brittle materials at room temperature. However, the defects that can result from the thermal cycling might self-heal at elevated temperature. Glass ceramic sealants of GC-H series and GC-B contain different amounts crystalline phases (20–95%). Furthermore the GC-H series have a lower sealing temperature (850 °C) than the GC-B (950 °C), hence different self-healing temperatures have been used for these materials of 850–900 °C and 900–950 °C, respectively. For example, the GC-H series specimens were first annealed at 850 °C for 24 h, and then after re-examination of the indentation marks, at 900 °C for 24 h. Fig. 9 displays the self-healing test for GC-HYSZ and GC-HZYBF. Fig. 9 shows that the cracks have not disappeared completely, but illustrate a limited degree of self-healing. The crack generated in the YSZ particle region disappeared after reheating.

Fig. 10 displays an impression in GC-B aged 500 h at room temperature and afterwards annealed at 950 °C for 24 h. The main radial crack remains, while the small crack branch disappeared. It appears that the lower amount of glassy phase

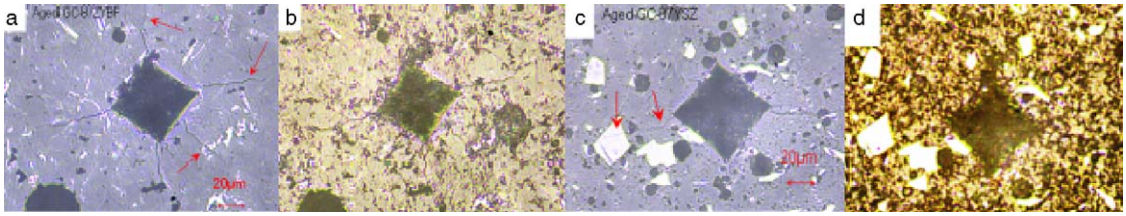

Fig. 9. Micrographs of indentations (10 N) for (a) aged GC-HYSZ before and (b) after self-healing at 900 °C/24 h, (c) aged GC-HZYBF before and (d) after self-healing at 900 °C/24 h.

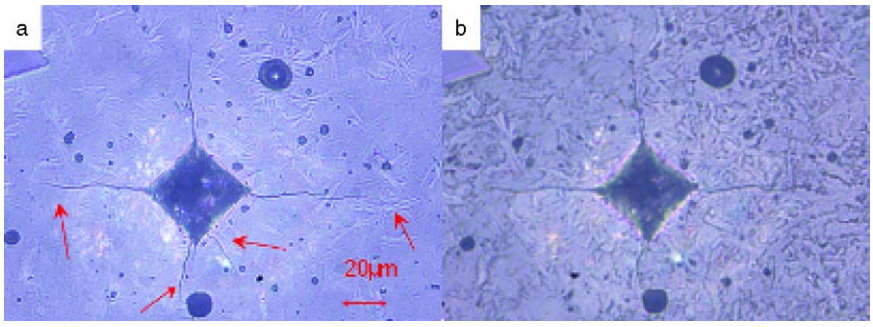

Fig. 10. Self-healing of aged GC-B (a) initial indentation (10 N) and (b) after 24 h at 950 °C.

in the GC-B specimen leads to the reduction of the healing rate comparing with GC-H series. The self-healing experiment suggests that the re-crystallization effect is much stronger than the self-healing due to viscous flow of the glass.

4. Conclusions

Glass ceramics are widely used as sealants for planar SOFC stacks. Due to the high requirements on the reliability, the mechanical properties of these materials need to receive considerable attention. Hardness, elastic modulus and fracture toughness of different Ba–Ca–Al-silicate sealant materials are reported. Limits of the elastic moduli are approximately 70 and 90 GPa, for the hardness the limits are around 4 and 8 GPa, the limits of the fracture toughness are about 0.6 and 1.5 MPa $m^{0.5}$. The effect of progressive crystallization and especially the toughness and ductility of the different filler materials is highlighted. The materials show at 40 °C under wet atmosphere evidence of slow crack growth. The self-healing experiments suggest that the re-crystallization effect is much stronger than the self-healing due to viscous flow of the glass. In the SOFC stacks during the thermal cycling, small cracks and defects may be generated in the sealant due to the tensile stresses caused by the CTE mismatch between different layers of the SOFC composite. However, only very small defects can be healed by the reheating.

References

1. Smeacetto F, Salvo M, D'Hérin Bytner FD, Leone P, Ferraris M. New glass and glass–ceramic sealants for planar solid oxide fuel cells. *J Eur Ceram Soc* 2009;**30**:933–40.
2. Mahapatra MK, Lu K. Glass-based seals for solid oxide fuel and electrolyzer cells—a review. *Mater Sci Eng R* 2010;**67**:65–85.
3. Gross S-M, Koppitz T, Remmel J, Reisgen U. Glass-ceramic materials of the system BaO–CaO–SiO_2 as sealants for SOFC applications. *Ceram Eng Sci Proc* 2005;**26/4**:239.
4. Ghosha S, Kundua P, Das Sharmaa A, Basu RN. Microstructure and property evaluation of barium aluminosilicate glass–ceramic sealant for anode-supported solid oxide fuel cell. *J Eur Ceram Soc* 2008;**28**:69–76.
5. Malzbender J, Steinbrech RW. Advanced measurement techniques to characterize thermo-mechanical aspects of solid oxide fuel cells. *J Power Sources* 2007;**173**:60–7.
6. Bahadur D, Lahl N, Singh K, Singheiser L, Hilpert K. Influence of nucleating agents on the chemical interaction of MgO–Al_2O_3–SiO_2–B_2O_3 glass sealants with components of SOFCs. *J Electrochem Soc* 2004;**151**:A558–62.
7. Meinhardt KD, Kim D-S, Chou Y-S, Weil KS. Synthesis and properties of a barium aluminosilicate, solid oxide fuel cell glass–ceramic sealant. *J Power Sources* 2008;**182**:188–96.
8. Malzbender J, den Toonder JMJ, Balkenende AR, de With G. A methodology to determine the mechanical properties of thin films, with application to nano-particle filled methyltrimethoxysilane sol–gel coatings. *Mater Sci Eng Rep* 2002;**36**:47.
9. Mencik J. *Strength and fracture of glass and ceramics*. Elsevier; 1992.
10. Nielsen KA, Solvang M, Nielsen SBL, Dinesen AR, Beeaff D, Larsen PH. Glass composite seals for SOFC application. *J Euro Ceram Soc* 2007;**27**:1817–22.